Materials Chemistry and Physics 217 (2018) 451–456

Contents lists available at ScienceDirect

Materials Chemistry and Physics

journal homepage: www.elsevier.com/locate/matchemphys

Effect of hydrothermal conditions on superconductivity and magnetism in $[Li_{1-x}Fe_xOH]FeS$

E. McDonnell, S. Jaszewski, H.-Y. Yang, M. Abramchuk, Fazel Tafti*

Department of Physics, Boston College, Chestnut Hill, MA 02467, USA

HIGHLIGHTS

- Hydrothermal synthesis of $[Li_{1-x}Fe_xOH]FeS$ requires temperatures between 150 to 180 °C
- Synthesis at higher temperatures reduces the iron impurity
- Smaller impurity reduces the scattering rate and increases the superconducting Tc
- These findings explain the variation of Tc in $[Li_{1-x}Fe_xOH]FeS$ quantitatively
- Tc of the intercalated $[Li_{1-x}Fe_xOH]FeS$ does not increase above the Tc of FeS

ARTICLE INFO

Keywords:
intercalation
Hydrothermal
Superconductivity
Magnetism

ABSTRACT

Recent reports of superconductivity and magnetism in single crystals of $[Li_{1-x}Fe_xOH]FeS$ show unexplained variations in both superconducting and magnetic properties. We investigate the effect of hydrothermal growth conditions on these properties and find that increasing the growth temperature systematically increases the superconducting transition temperature (T_c), sharpens the magnetic transition, and decreases the scattering rate (Γ). The slow rate of T_c suppression with increasing Γ indicates a conventional *s*-wave superconducting state according to the Abrikosov-Gorkov expression. Samples with higher scattering rate show broader magnetic transitions and a stronger temperature dependence in the magnetic susceptibility. These results identify disorder, due to interstitial iron impurities, as the unique internal parameter responsible for the unexplained variations in T_c and magnetic ordering. We demonstrate the optimal hydrothermal growth conditions to minimize disorder and maximize T_c in $[Li_{1-x}Fe_xOH]FeS$ crystals.

1. Introduction

Mackinawite is a naturally occurring mineral of iron and nickel with the formula $(FeNi)_{1+x}S$ and a tetragonal unit cell in the space group *P4/nmm* [1]. Pure FeS crystallizes in two forms: the stable hexagonal phase (h-FeS) with a NiAs-type structure, and the metastable tetragonal phase (t-FeS) with an anti-PbO-type structure [2]. Recently, single crystals of the metastable t-FeS were grown using a hydrothermal method and found to be superconducting below 5 K [3,4]. The search for superconductivity in tetragonal iron sulfide with Mackinawite structure was motivated by the closely related tetragonal iron selenide (t-FeSe) which is also metastable and superconducting [5]. Whereas the stable hexagonal phase is not superconducting in both FeS and FeSe, the metastable tetragonal phase is superconducting.

The crystal structures of both t-FeS and t-FeSe are constructed from layers of edge-sharing iron-chalcogenide tetrahedra separated by a van der Waals gap of 2.6 and 2.4 Å respectively. Van der Waals materials provide an opportunity for intercalation experiments [6]. For example, the intercalation of t-FeSe with alkali metals (K [7], Rb [8], Cs [9]), alkali hydroxide (LiOH) [10,11], and alkali ethylenediamine $(A_x(C_2H_8N_2)_y)$ [12] drastically increases the T_c from 8 to 30 K. In contrast, an intercalant-independent T_c is observed in black phosphorous and MoS_2 [13–15]. Despite the structural and chemical similarities between t-FeS and t-FeSe, we report an intercalant-independent T_c in t-FeS. This contrasts with a prior work that reported an increase of T_c due to intercalation and a significant variation of superconducting and magnetic properties between different samples of $[Li_{1-x}Fe_xOH]FeS$ [16]. Here, we demonstrate that the random variations of T_c in $[Li_{1-x}Fe_xOH]FeS$ can be quantitatively explained by different disorder levels. This analysis places an upper bound to the T_c of $[Li_{1-x}Fe_xOH]FeS$ that does not exceed the T_c of t-FeS. We demonstrate that hydrothermal conditions determine the disorder level which in turn affects

* Corresponding author.
E-mail address: fazel.tafti@bc.edu (F. Tafti).

https://doi.org/10.1016/j.matchemphys.2018.06.018
Received 31 October 2017; Received in revised form 5 June 2018; Accepted 9 June 2018
Available online 22 June 2018
0254-0584/

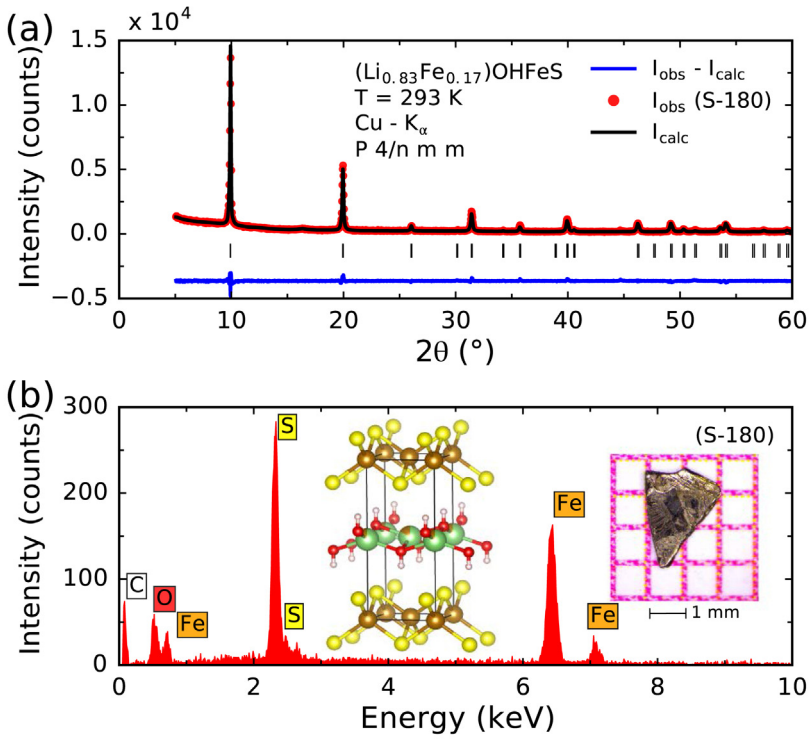

Fig. 1. (a) Powder x-ray diffraction pattern of the sample S-180 grown at 180 °C in the autoclave. The solid black line shows the Rietveld refinement calculation. The blue line shows the difference between calculated and observed intensities. The quoted value $x = 0.17$ is determined by the best Rietveld fit. (b) EDX results from S-180 confirm the presence of Fe, O, and S with the ratio Fe:S = 1.31 (8):1 in qualitative agreement with the X-ray results. The crystal structure of $[Li_{1-x}Fe_xOH]FeS$ is illustrated in the inset and a picture of the crystal is shown on millimeter paper. (For interpretation of the references to colour in this figure legend, the reader is referred to the Web version of this article.)

the superconducting and magnetic properties of $[Li_{1-x}Fe_xOH]FeS$. Finally, we use band structure calculations to show that intercalation with LiOH does not dope the t-FeS system which explains the intercalant-independent T_c.

2. Experimental methods

2.1. Crystal growth

$[Li_{1-x}Fe_xOH]FeS$ single crystals were prepared through a cation-exchange reaction between LiOH(*aq*) and $K_{0.8}Fe_2S_2$(*s*) under hydrothermal conditions [16]. The process consisted of three steps: solid state synthesis of h-FeS, flux growth of $K_{0.8}Fe_2S_2$, and hydrothermal growth of $[Li_{1-x}Fe_xOH]FeS$. To synthesize h-FeS, iron powder (Fe, Alfa Aesar, 99.9%) and sulfur pieces (S, Strem Chemicals, 99.999%) with a 1:1 mole ratio and 1.0 g total mass were mixed and placed in a quartz tube inside an argon-filled glovebox (O_2 and H_2O contents < 0.1 ppm). The tube was then flame sealed under vacuum. The reactants were heated to 500 °C at 1 °C/min, held at 500 °C for 8 h, heated to 850 °C at 1 °C/min, held at 850 °C for 18 h, then cooled to room temperature at 5 °C/min. To grow $K_{0.8}Fe_2S_2$ crystals, potassium chunks (K, Alfa Aesar, 98%) and h-FeS powder with a 1:2 mole ratio and 1.2 g total mass were combined and placed in a quartz tube inside the glovebox. The tube was then flame sealed under vacuum inside a larger tube to protect against potassium-induced corrosion of quartz. The reactants were heated to 1030 °C at 1.7 °C/min, held at 1030 °C for 3 h, slowly cooled to 650 °C at 0.1 °C/min, and furnace cooled to room temperature. For the Hydrothermal growth of $[Li_{1-x}Fe_xOH]FeS$ crystals, several $K_{0.8}Fe_2S_2$ crystals with 0.3 g total mass were combined with 72 mmol lithium hydroxide monohydrate ($LiOH{\cdot}H_2O$, Alfa Aesar, 98%), 3 mmol iron powder (Fe, Alfa Aesar, 99.9%), 3 mmol lithium sulfide (Li_2S, Alfa Aesar, 99.9%) or thiourea ($SC(NH_2)_2$, Sigma Aldrich, 99%) as the sulfur source, and 1 mmol tin granules (Sn, Alfa Aesar, 99.9%). The feedstock was loaded into a 10 ml Teflon-lined Parr autoclave filled with de-ionized water at 90% filling fraction inside a nitrogen-filled glovebox (O_2 and H_2O contents < 0.1 ppt). In the hot and concentrated basic environment of the autoclave, the tin granules form $[Sn(OH)_6]^{2+}$ while evolving H_2 gas [17]. This provides a stronger reducing environment that promotes the intercalation of $K_{0.8}Fe_2S_2$ with LiOH [18]. Four attempts were made with the autoclave heated to 110, 120, 150, and 180 °C and held at constant temperature for 3 days. After each attempt, the final products were washed with de-ionized water, filtered, and dried under vacuum.

2.2. Measurements

Powder X-ray Diffraction (PXRD) data were collected in a Bruker D8 ECO instrument in the Bragg-Brentano geometry with a copper X-ray source (Cu-Kα), a nickel filter to absorb the Kβ radiation, and two 2.5° Soller slits after the source and before the LYNXEYE XE 1D energy dispersive detector. Rietveld refinement on the PXRD pattern was performed using the FullProf suite [19]. Peak shapes were modeled with the Thompson-Cox-Hastings pseudo-Voigt profile convoluted with axial divergence asymmetry. Energy Dispersive X-ray Spectroscopy (EDX) was performed with an EDAX detector installed on a JEOL field emission electron microscope (FESEM). DC Magnetization was measured as a function of field and temperature in a 7 T Quantum Design MPMS3 system. A low background sapphire holder inside a plastic straw was used to mount the crystals with field parallel to the $c-$axis. Four probe resistivity measurements and heat capacity measurements were performed in a 9 T Quantum Design Dynacool system.

3. Results and discussion

3.1. Material characterizations

A previous report on $[Li_{1-x}Fe_xOH]FeS$ with the nominal x = 0.17 showed unexplained variations in the superconducting transition T_c, the magnetic transition T_N, and the residual resistivity ρ_0 of different samples [16]. To understand these variations, we attempted four hydrothermal growth cycles at T = 110, 120, 150, and 180 °C, with the resulting samples labeled S-110, S-120, S-150, and S-180. T_c varied

Table 1
Crystallographic data for $[Li_{1-x}Fe_xOH]FeS$ obtained at room temperature using Cu-Kα radiation with λ = 1.5406 Å. Unit cell parameters and Rietveld calculation factors are reported. The isotropic Debye-Waller (thermal) factor B_{iso} is less than one for Fe and S.

Unit cell parameters		Refinement parameters	
Space Group	*P4/nmm*	B_{iso} (Å^2)	< 1.0
a (Å)	3.70087 (8)	R_F (%)	11.14
c (Å)	8.88824 (6)	R_{wp} (%)	22.2
V (Å^3)	121.737 (8)	R_{exp} (%)	16.99
Z	2	χ^2	1.7

from batch to batch and even within the same batch, similar to the previous report [16]. However, we found that increasing the synthesis temperature systematically reduced such sample variations within the same batch and improved T_c.

Fig. 1(a) shows the PXRD pattern of S-180 indexed in the space group 129 (*P4/nmm*), the same space group as t-FeS or t-FeSe. The crystal size and the PXRD do not show visible differences in the crystallinity of samples grown at different temperatures. As shown in the inset of Fig. 1(b), the crystals are large, layered, and easy to cleave. The tetragonal unit cell of $[Li_{1-x}Fe_xOH]FeS$ is illustrated in the inset of Fig. 1(b) with layers of edge-sharing FeS_4 tetrahedra separated by $[Li_{1-x}Fe_xOH]$ molecules. Unit cell parameters and refinement *R*-factors are presented in Table 1. Wykoff positions are listed in Table 2. The ratio Fe/S = 1.17 from PXRD refinement is consistent with Fe/S = 1.31 (8) from EDX as shown in Fig. 1(b). Due to the presence of the light elements lithium and oxygen, the EDX analysis is expected to differ slightly from the refinement model. The statistical error is derived from measuring EDX on several samples. We performed EDX measurements on representative samples grown at different temperatures and realized that the Fe/S ratio increases from 1.31 (8) to 1.52 (6) and 1.72 (8) in samples grown at 180 °C (S-180), 150 °C (S-150), and 110 °C (S-110) respectively. This shows qualitatively that the iron content (*x*) in $[Li_{1-x}Fe_xOH]FeS$ increases with decreasing growth temperature so there will be more iron atoms substituting for lithium in the intercalant $[Li_{1-x}Fe_xOH]$. These iron impurities act as scattering centers for electrons in the normal state and for cooper pairs in the superconducting state.

3.2. Superconducting properties

The scattering effect of iron impurities on electrons and cooper pairs is studied by measuring the electrical transport. Fig. 2(a) shows the temperature dependence of resistivity in three representative samples: S-110, S-150, and S-180 grown at 110, 150, and 180 °C. Due to the layered structure of the material, it is difficult to accurately determine the sample dimensions, especially the thickness, which are required to convert electrical resistance to resistivity. Therefore, the resistivity of all samples is normalized to the average value of 4 mΩ cm at room temperature. Solid lines on each data set in Fig. 2(a) are fits to the expression $\rho = AT^2 + BT + \rho_0$. The residual resistivity (ρ_0) systematically decreases with increasing the growth temperature indicating less iron impurity in S-180 compared to S-150 and S-110. Higher temperatures in the autoclave increase the solubility of the feedstock and promote the intercalation with LiOH and less iron impurity.

Table 2
Wykoff sites, atomic coordinates, and site occupancies reported for the crystal structure of $[Li_{1-x}Fe_xOH]FeS$.

atom	site	*x*	*y*	*z*	occupancy
H1	2c	1/4	1/4	0.66000	1.0
O1	2c	1/4	1/4	0.5700 (5)	1.0
Li1	2b	3/4	3/4	1/2	0.833 (3)
Fe1	2b	3/4	1/4	1/2	0.16 (7)
Fe2	2a	3/4	1/4	0	1.0
S2	2c	1/4	1/4	0.1484 (5)	1.0

The pair-braking effect of iron impurities is observed in Fig. 2(b) that magnifies the region of superconducting transition and shows that samples with smaller ρ_0 have higher T_c. Since ρ_0 is determined by the scattering rate Γ, Fig. 2(b) suggests a link between Γ and T_c. This link will be quantitatively analyzed later.

Fig. 2(c) shows that the superconducting transition shifts to lower temperatures with increasing magnetic field in sample S-180. Similar behavior is observed in other samples. By taking the midpoint of the transition as T_c at each field, an *H-T* phase diagram is produced in Fig. 2(d) with a fit to the Werthamer-Helfand-Hohenberg expression:

$$H_{c2}(T) = H_{c2}(0)\left[1 - \frac{1}{2\alpha}\left(\frac{T}{T_c}\right)^2\right] \quad (1)$$

where α is a constant between 0.69 (dirty limit) and 0.72 (clean limit) [20]. From this fit, the zero temperature upper critical field $H_{c2}(0)$ is approximately 400 Oe. $H_{c2}(0)$ is two orders of magnitude less than the Pauli limit for $[Li_{1-x}Fe_xOH]FeS$ according to the estimation $H_P \approx 1.85T_c \approx 4.6$ T. Therefore, the pairing wave function must be spin-singlet – that is either *s*-wave or *d*-wave [21]. These two possibilities can be distinguished by studying the relation between the scattering rate (Γ) and T_c.

3.3. Abrikosov-Gorkov analysis

To quantify the link between Γ and T_c, we characterized 9 samples from batches grown at different temperatures. For each sample, T_c was determined from the midpoint of the resistive transition and the scattering rate was determined from the relaxation time ($\Gamma = 1/2\tau$). The relaxation time for each sample was calculated using the single band Drude model, $\rho_0 = m/ne^2\tau$, where the carrier concentration was obtained from the Hall coefficient ($R_H = 1/ne$). Fig. 3(a) shows a weak temperature dependence in the Hall coefficient with $R_H = 0.06$ cm^3/C at $T = 0$ corresponding to hole-like carriers with a concentration $n = 1.04 \times 10^{20}$ cm^{-3}. From here, the Fermi wave vector can be calculated using the expression $k_F = (3\pi^2 n)^{1/3}$, which gives $k_F = 1.46 \times 10^7$ cm^{-1}, assuming a spherical Fermi surface. Fig. 3(b) shows the molar heat capacity for the same sample which can be used to extract the effective mass of carriers. According to the Sommerfeld-Debye model, heat capacity is given by the expression $C/T = \gamma + \beta T^2$, where $\gamma = \frac{\pi^2}{2}N\frac{k_B^2}{E_F}$ and $\beta = \frac{12\pi^4}{5}rNk_B\Theta_D^{-3}$ [23]. Here E_F is the Fermi energy, *N* is the Avogadro number, *r* is the number of atoms per molecule, and Θ_D is the Debye temperature. Using k_F from the Hall effect, we calculate $\gamma = 0.044$ J/mol K^2 which is smaller than the experimental value reported on Fig. 3(b). The ratio between the observed and the calculated γ gives the effective mass of carriers $m^* = \gamma_{exp}/\gamma_{cal} = 0.34m_e$.

Using the effective mass from heat capacity and the carrier concentration from the Hall effect, we can calculate the scattering rate from the expression $\Gamma = e\rho_0/2\,m^*R_H$ for each sample with a specific ρ_0. The Abrikosov-Gorkov (A-G) formula [24–26] describes the variation of T_c with Γ

$$\ln\left(\frac{T_{c0}}{T_c}\right) = \Psi\left(\frac{1}{2} + \frac{\hbar\Gamma}{2\pi k_B T_c}\right) - \Psi\left(\frac{1}{2}\right) \quad (2)$$

where T_{c0} is the superconducting transition for ideally pure material and Ψ is the digamma function. Fig. 3(c) shows that samples grown at higher temperatures have lower Γ and higher T_c. This is consistent with a smaller *x* in $[Li_{1-x}Fe_xOH]FeS$ samples grown at higher temperatures as explained in Section 3.1. The excessive iron in the intercalant $[Li_{1-x}Fe_xOH]$ is the source of scattering in $[Li_{1-x}Fe_xOH]FeS$.

The maximum possible T_c in $[Li_{1-x}Fe_xOH]FeS$ from this analysis is $T_{c0} = 2.9$ K. Our highest quality samples with $T_c = 2.6$ K are grown

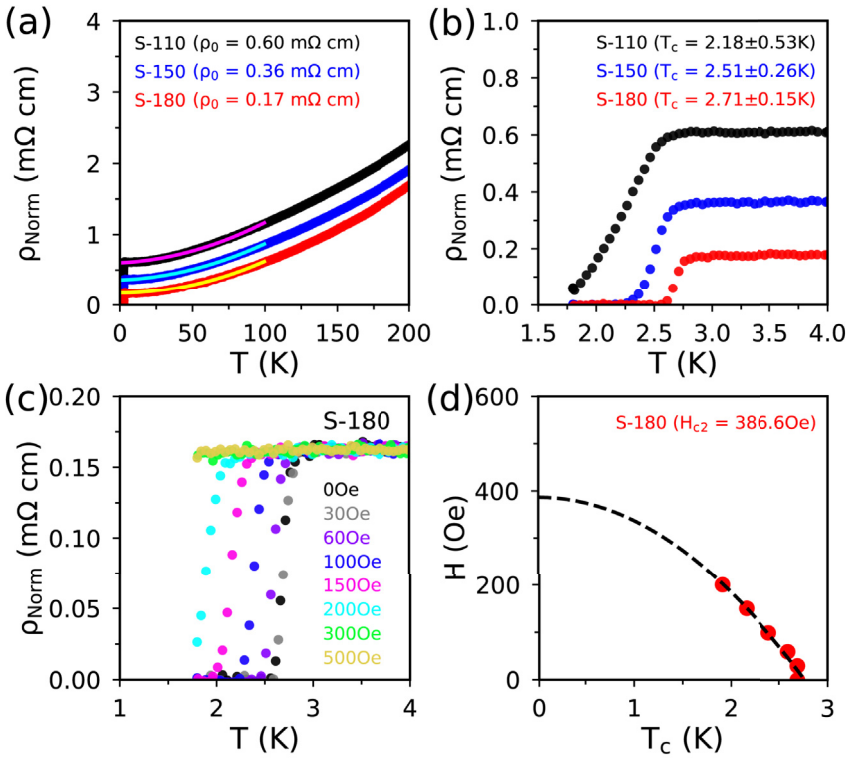

Fig. 2. (a) Resistivity of three $[Li_{1-x}Fe_xOH]FeS$ samples grown at 110, 150, and 180 °C. These samples are labeled S-110 (black data), S-150 (blue), and S-180 (red). Solid lines are fits to the expression $\rho = AT^2 + BT + \rho_0$. S-180, the sample grown at 180 °C, has the lowest residual resistivity ρ_0 whereas S-110 has the highest ρ_0. (b) Resistivity plotted as a function of temperature below 4 K, showing that samples with lower residual resistivity have higher T_c. (c) $\rho(T)$ from sample S-180 measured at several different magnetic fields. T_c decreases with increasing field. We define T_c as the mid-point of the transition and use the width of the transition as the uncertainty in T_c. (d) T_c values at different H are used to draw the H-T_c phase diagram of sample S-180 with $H_{c2} = 386.6$ Oe.

using thiourea as the sulfur source at 180 °C (Fig. 3(c)). We do not observe $T_c = 6$ K as reported in Ref. [16] for intercalated samples in the presence of thiourea. According to our observations, the critical temperature of $[Li_{1-x}Fe_xOH]FeS$ does not exceed the T_c of t-FeS.

The rate of T_c suppression by Γ can be used as an indirect probe of the pairing symmetry in superconductors. Disorder has a strong pair-braking effect on superconductors with sign changing order parameters such as d or $s^{\pm}$ states [24–26]. In these cases, T_c will be completely suppressed at $\Gamma \sim \Gamma_c = 2\pi k_B T_{c0}/h$ [27,28]. For example, KFe_2As_2 with $T_{c0} = 3.9$ K has a sign-changing (possibly d-wave) superconducting order parameter [22]. As a result, superconductivity completely vanishes at $\Gamma/\Gamma_c \sim 1$ in KFe_2As_2. Fig. 3(c) shows a slower rate of T_c suppression in $[Li_{1-x}Fe_xOH]FeS$ compared to KFe_2As_2. Therefore, the pairing symmetry in $[Li_{1-x}Fe_xOH]FeS$ is most likely a conventional

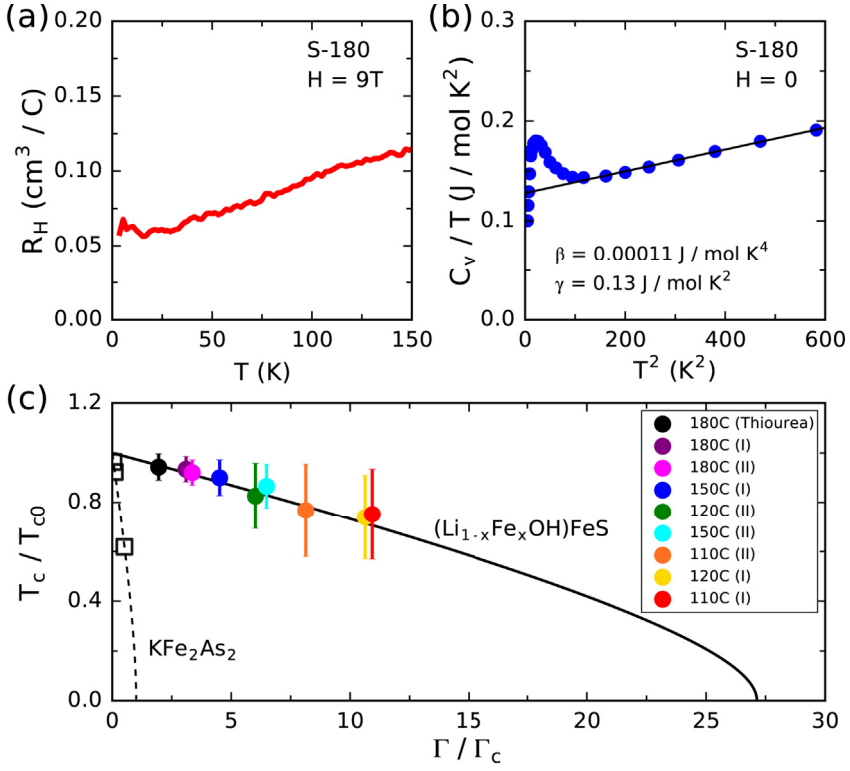

Fig. 3. (a) Hall effect as a function of temperature from 2 to 150 K in a $[Li_{1-x}Fe_xOH]FeS$ sample grown at 180 °C labeled as S-180. The data are taken at positive and negative 9 T and antisymmetrized to calculate R_H. (b) Heat capacity plotted as C/T versus T^2 from 2 to 25 K in the sample S-180. The peak in C/T corresponds to the magnetic transition at 8 K. From the linear fit $C/T = \beta + \gamma T^2$, we derive the effective mass and the Debye temperature as explained in the text. (c) The Abrikosov-Gorkov analysis is performed for $[Li_{1-x}Fe_xOH]FeS$ by plotting normalized T_c as a function of normalized scattering rate for nine samples. Hydrothermal growth temperature for each sample is specified in the legend. These data follow the AG expression (Eq. (2)) traced with a solid black line. The same analysis is done for KFe_2As_2 where the data are taken from Ref. [22] and the A-G expression is traced with a dashed line. T_c suppression occurs at $\Gamma \sim \Gamma_c$ in KFe_2As_2 compared to $\Gamma \gg \Gamma_c$ in $[Li_{1-x}Fe_xOH]FeS$.

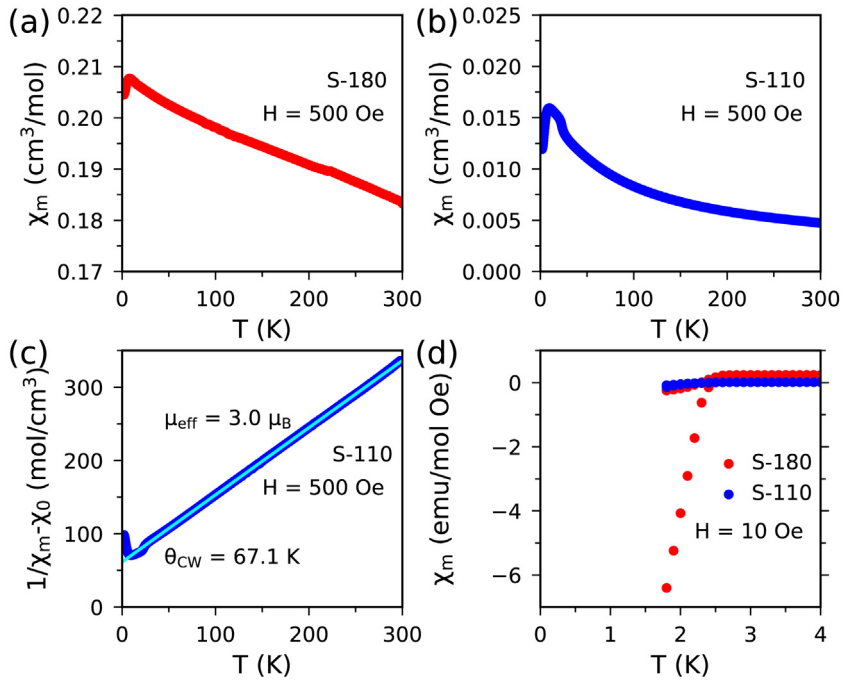

Fig. 4. (a) Molar susceptibility in the $[Li_{1-x}Fe_xOH]FeS$ sample S-180 (made at 180°C) shows a weak temperature dependence and a sharp peak at $T_N = 8$ K. (b) Molar susceptibility in S-110 (made at 110°C) shows a stronger temperature dependence and a broad peak extending from 8 to 22 K. (c) Curie-Weiss analysis for S-110 gives effective moment $\mu_{eff} = 3\mu_B$ close to the value expected from Fe^{2+} in a tetrahedral coordination. From this analysis, the Curie-Weiss temperature is $\Theta_{CW} = 67.1$ K. (d) The superconducting transition in the susceptibility channel corresponds to 80% volume fraction in the clean sample (S-180) and 10% volume fraction in the disordered sample (S-110).

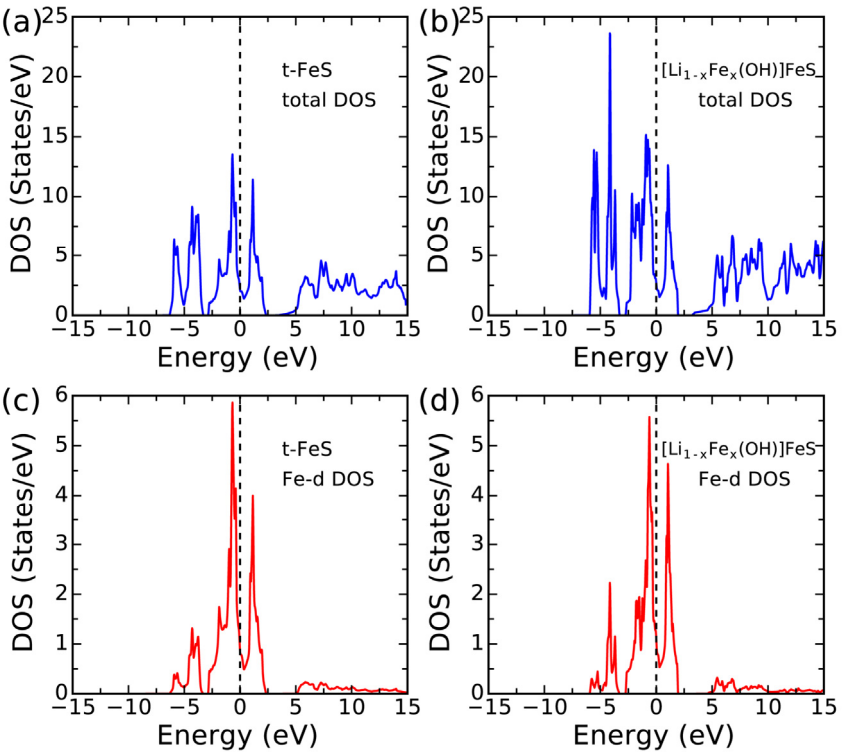

Fig. 5. (a) Total density of states in t-FeS. The two peaks below and above E_F are Van Hove singularities. (b) Total density of states (DOS) in $[Li_{1-x}Fe_xOH]FeS$. A similar DOS is observed before and after intercalation of t-FeS. Therefore, intercalation does not dope the system with extra carriers and does not enhance T_c. (c) Projected DOS on the *d*-orbitals of iron in t-FeS. The partial DOS from iron atoms has a dominant effect on superconductivity. (d) Projected DOS on the *d*-orbitals of iron in $[Li_{1-x}Fe_xOH]FeS$. A similar DOS is observed before and after intercalation confirming a lack of doping effect.

isotropic *s*-wave instead of $s^{\pm}$ or *d*-wave.

3.4. Magnetic properties

Fig. 4(a) compares the temperature dependence of the magnetic susceptibility $\chi(T)$ in two $[Li_{1-x}Fe_xOH]FeS$ samples grown at 180 and 110 °C. A sharp transition is observed at $T_N = 8$ K in the clean sample S-180, whereas a broad transition is observed between 8 and 22 K in the disordered sample S-110. In the clean sample S-180, $\chi(T)$ shows a weak temperature dependence (Pauli behavior) at $T > T_N$ characteristic of itinerant moments. In the disordered sample S-110, $\chi(T)$ shows a stronger temperature dependence (Curie-Weiss behavior) characteristic of localized moments. The change of behavior from itinerant magnetism and sharp transition in the clean sample to localized magnetism and broad transition in the disordered sample confirms the impact of the scattering rate Γ on the magnetic behavior of $[Li_{1-x}Fe_xOH]FeS$. Fig. 4(c) shows the data in S-110 fitted to the Curie-Weiss (CW) expression, $\chi - \chi_0 = C/(T - \Theta_{CW})$, where χ_0 is a background and Θ_{CW} is the CW temperature. The effective moment from the CW fit ($\mu = 3\mu_B$) is close to the value expected from Fe^{2+} in the tetrahedral coordination

($2.8\mu_B$). Fig. 4(d) compares the superconducting transition between S-110 and S-180. The estimated superconducting volume fraction is 80% in S-180 and 10% in S-110.

3.5. Density of states

As mentioned in the introduction, intercalation of t-FeSe with LiOH increases T_c from 8 to 30 K [10]. However, the intercalation of t-FeS with LiOH does not increase the T_c. In fact, T_c decreases with intercalation due to the impurity scattering from extra iron atoms in the intercalant [$Li_{1-x}Fe_xOH$]. We performed DFT calculations on both t-FeS and [$Li_{1-x}Fe_xOH$]FeS to explain the intercalant-independent T_c. Fig. 5(a) shows two peaks in the total density of state (DOS) corresponding to Van Hove singularities below and above the Fermi energy in t-FeS. Fig. 5(b) shows that neither of these peaks crosses E_F in the intercalated system [$Li_{1-x}Fe_xOH$]FeS, i.e. intercalation with LiOH does not dope the t-FeS system. Fig. 5(c) and (d) show the same comparison between t-FeS and [$Li_{1-x}Fe_xOH$]FeS based on the density of iron *d*-states instead of total DOS. If the intercalation had a doping effect, one of the peaks would have crossed E_F as a result of intercalation, and the accumulation of states at E_F would have considerably increased T_c. Therefore, the intercalant-independent T_c in [$Li_{1-x}Fe_xOH$]FeS is due to a lack of doping effect.

4. Conclusions

We investigated the effect of hydrothermal growth conditions on the superconducting and magnetic properties of [$Li_{1-x}Fe_xOH$]FeS. Hydrothermal growth at higher temperatures systematically produced samples with less iron impurity, smaller scattering rates, and consequently, smaller residual resistivity (Fig. 2). The Abrikosov-Gorkov analysis (Eq. (2)) confirmed impurity scattering as the intrinsic parameter that controls T_c. From this analysis, the superconducting wave function appears to have a conventional *s*-wave symmetry. By increasing the scattering rate, the magnetic behavior of [$Li_{1-x}Fe_xOH$]FeS drastically changed from sharp magnetic transitions and itinerant moments in clean samples to broad transitions and localized moments in disordered samples. Therefore, the unexplained sample dependent properties [16] of [$Li_{1-x}Fe_xOH$]FeS were explained in a unified picture where disorder controls the T_c, the superconducting volume fraction, and the magnetic behavior of the material. The optimal conditions to grow single crystals of [$Li_{1-x}Fe_xOH$]FeS were at $T = 180$ °C and with thiourea as the sulfur source.

Acknowledgments

This work was funded by BC startup budget and the National Science Foundation, award No. DMR-1708929.

References

[1] J.W. Anthony, R.A. Bideaux, K.W. Bladh, M.C. Nichols, Handbook of Mineralogy, Elements, Sulfides and Sulfosalts, Mineral Data Pub, Tucson, Ariz, 1990.
[2] E. F. Bertaut, P. Burlet, J. Chappert, Sur l'absence d'ordre magnetique dans la forme quadratique de FeS, Solid State Commun., 3(10) 335–338.
[3] X. Lai, H. Zhang, Y. Wang, X. Wang, X. Zhang, J. Lin, F. Huang, Observation of superconductivity in tetragonal FeS, J. Am. Chem. Soc. 137 (32) (2015) 10148–10151.
[4] C.K.H. Borg, X. Zhou, C. Eckberg, D.J. Campbell, S.R. Saha, J. Paglione, E.E. Rodriguez, Strong anisotropy in nearly ideal tetrahedral superconducting FeS single crystals, Phys. Rev. B 93 (9) (2016) 094522.
[5] U. Patel, J. Hua, S.H. Yu, S. Avci, Z.L. Xiao, H. Claus, J. Schlueter, V.V. Vlasko-Vlasov, U. Welp, W.K. Kwok, Growth and superconductivity of FeSex crystals, Appl. Phys. Lett. 94 (8) (2009) 082508.
[6] Y. Jung, Y. Zhou, J.J. Cha, Intercalation in two-dimensional transition metal chalcogenides, Inorg. Chem. Front. 3 (4) (2016) 452–463.
[7] J. Guo, S. Jin, G. Wang, S. Wang, K. Zhu, T. Zhou, M. He, X. Chen, Superconductivity in the iron selenide $K_xFe_2Se_2$ ($0 \le x \le 1.0$), Phys. Rev. B 82 (18) (2010) 180520.
[8] A.F. Wang, J.J. Ying, Y.J. Yan, R.H. Liu, X.G. Luo, Z.Y. Li, X.F. Wang, M. Zhang, G.J. Ye, P. Cheng, Z.J. Xiang, X.H. Chen, Superconductivity at 32 K in single-crystalline $RbxFe_{2-y}Se_2$, Phys. Rev. B 83 (6) (2011) 060512.
[9] A. Krzton-Maziopa, Z. Shermadini, E. Pomjakushina, V. Pomjakushin, M. Bendele, A. Amato, R. Khasanov, H. Luetkens, K Conder, Synthesis and crystal growth of $Cs_{0.8}(FeSe)_{0.982}$: a new iron-based superconductor with T c = 27 K, J. Phys. Condens. Matter 23 (5) (2011) 052203.
[10] X.F. Lu, N.Z. Wang, H. Wu, Y.P. Wu, D. Zhao, X.Z. Zeng, X.G. Luo, T. Wu, W. Bao, G.H. Zhang, F.Q. Huang, Q.Z. Huang, X.H. Chen, Coexistence of superconductivity and antiferromagnetism in (Li0.8Fe0.2)OHFeSe, Nat. Mater. 14 (3) (2015) 325–329.
[11] X. Dong, H. Zhou, H. Yang, J. Yuan, K. Jin, F. Zhou, D. Yuan, L. Wei, J. Li, X. Wang, G. Zhang, Z. Zhao, Phase diagram of $(Li_{1-x}Fe_x)$OHFeSe: a bridge between iron selenide and arsenide superconductors, J. Am. Chem. Soc. 137 (1) (2015) 66–69.
[12] T. Noji, T. Hatakeda, S. Hosono, T. Kawamata, M. Kato, Y. Koike, Synthesis and post-annealing effects of alkaline-metal-ethylenediamine-intercalated superconductors $A_x(C_2H_8N_2)_yFe_{2-z}Se_2$ (A = Li, Na) with $T_c = 45$ K, Physica C: Supercond. Appl. 504 (2014) 8–11.
[13] R. Zhang, J. Waters, A.K. Geim, I.V. Grigorieva, Intercalant-independent transition temperature in superconducting black phosphorus, Nat. Commun. 8 (2017) 15036.
[14] Gonzalo Abellán, Christian Neiss, Vicent Lloret, Stefan Wild, C. Chacón-Torres Julio, Katharina Werbach, Filippo Fedi, Hidetsugu Shiozawa, Andreas Görling, Herwig Peterlik, Thomas Pichler, Frank Hauke, Andreas Hirsch, Exploring the formation of black phosphorus intercalation compounds with alkali metals, Angew. Chem. Int. Ed. 56 (48) (2017) 15267–15273.
[15] R. Zhang, I.-L. Tsai, J. Chapman, E. Khestanova, J. Waters, I.V. Grigorieva, Superconductivity in potassium-doped metallic polymorphs of MoS_2, Nano Lett. 16 (1) (2016) 629–636.
[16] X. Zhou, C. Eckberg, B. Wilfong, S.-C. Liou, H.K. Vivanco, J. Paglione, E.E. Rodriguez, Superconductivity and magnetism in iron sulfides intercalated by metal hydroxides, Chem. Sci. 8 (5) (2017) 3781–3788.
[17] P.J. Smith (Ed.), Chemistry of Tin, second ed., Springer Netherlands, 1998.
[18] X. Zhou, C.K.H. Borg, J.W. Lynn, S.R. Saha, J. Paglione, E.E. Rodriguez, The preparation and phase diagrams of $(^7Li_{1-x}Fe_xOD)$FeSe and $(Li_{1-x}Fe_xOH)$FeSe superconductors, J. Mater. Chem. C 4 (18) (2016) 3934–3941.
[19] J. Rodriguez-Carvajal, Recent advances in magnetic structure determination by neutron powder diffraction, Phys. B Condens. Matter 192 (1) (1993) 55–69.
[20] N.R. Werthamer, E. Helfand, P.C. Hohenberg, Temperature, Purity, Dependence of the superconducting critical field, H_{c2}. Iii. Electron spin and spin-orbit effects, Phys. Rev. 147 (1) (1966) 295–302.
[21] M. Tinkham, Introduction to Superconductivity: second ed., 2nd Edition, Dover Publications.
[22] J.-P. Reid, M.A. Tanatar, A. Juneau-Fecteau, R.T. Gordon, S.R. de Cotret, N. Doiron-Leyraud, T. Saito, H. Fukazawa, Y. Kohori, K. Kihou, C.H. Lee, A. Iyo, H. Eisaki, R. Prozorov, L. Taillefer, Universal heat conduction in the iron arsenide superconductor KFe_2As_2: evidence of a *d* -wave state, Phys. Rev. Lett. 109 (8) (2012) 087001.
[23] N.W. Ashcroft, N.D. Mermin, Solid State Physics, first ed., Brooks Cole, New York, 1976.
[24] P.J. Hirschfeld, P. Wölfle, D. Einzel, Consequences of resonant impurity scattering in anisotropic superconductors: thermal and spin relaxation properties, Phys. Rev. B 37 (1) (1988) 83–97.
[25] R.J. Radtke, K. Levin, H.-B. Schüttler, M.R. Norman, Predictions for impurity-induced T_c suppression in the high-temperature superconductors, Phys. Rev. B 48 (1) (1993) 653–656.
[26] S. Graser, P.J. Hirschfeld, L.-Y. Zhu, T. Dahm, Tc suppression and resistivity in cuprates with out of plane defects, Phys. Rev. B 76 (5) (2007) 054516.
[27] Y. Sun, K. Maki, Transport properties of D -wave superconductors with impurities, Europhys. Lett. 32 (4) (1995) 355.
[28] Y. Wang, A. Kreisel, P.J. Hirschfeld, V. Mishra, Using controlled disorder to distinguish $s \pm$ and $s++$ gap structure in Fe-based superconductors, Phys. Rev. B 87 (9) (2013) 094504.